Authenticating Edges Produced by Zero-Crossing Algorithms

JAMES J. CLARK, MEMBER, IEEE

Abstract—**It is shown that zero-crossing edge detection algorithms can produce edges which do not correspond to significant image intensity changes. Such edges are called phantom or spurious. A method for classifying zero crossings as corresponding to "authentic" or "phantom" edges is presented.**

The contrast of an authentic edge is shown to increase with decreasing filter scale (and hence higher resolution), and the contrast of phantom edges is shown to decrease with a decrease in the filter scale. Thus, a phantom edge is truly a phantom edge in that the closer one examines it the weaker it becomes.

The results of applying the classification schemes described in this paper to synthetic and authentic signals in one and two dimensions are given.

The significance of the phantom edges is examined with respect to their frequency and strength relative to the authentic edges, and it is seen that authentic edges are denser and stronger, on the average, than phantom edges.

Index Terms—**Edge authentication, edge detection, phantom edges, scale space.**

I. Introduction

A FUNDAMENTAL operation in early vision is that of the detection of changes in image intensities, sometimes referred to as *edge* detection. These edges are used by higher-level visual processes such as stereo and motion analysis and scene segmentation. These higher-level processes must assume that the edges supplied to them have physical significance. For example, in edge-based stereo vision algorithms (e.g., [8]), a search is made to find edges in two spatially disparate images that correspond to the same scene feature. Obviously, if the edges that are supplied to the stereo vision module do not have any physical significance (that is, are not tied to events in the scene, external to the camera and visual processing system), then the depth information obtained from these edges cannot be expected to be physically significant either.

A commonly used method for localizing edges in image intensities is to associate edges with the zero crossings of the second derivative (or a suitable second-order differential operator) of a smoothed version of the image [2], [7]. We show in this paper that these methods can produce phantom, or spurious, edges, which have no correspondence to significant changes in image intensity. It is seen that the phantom edges occur, for the domain of smoothed step edges, when two spatially consecutive edges have the same sense (i.e., dark to light or light to dark).

Given that an edge detector can produce phantom edges, one must be able to distinguish these edges from authentic edges, so that they may be discarded, and the remaining authentic edges can be used in higher-level visual processes. In this paper, we provide methods for performing this classification in one and two dimensions. These methods are seen to be related to the technique of *non-maximum suppression* [2].

Typically, the strength, or contrast, of the phantom zero crossings is observed to be less than that of the authentic zero crossings. They are also less frequent. In Section IV, we quantify the relative strength and frequency of authentic and nonauthentic edges for the case of normally distributed random one-dimensional signals and compare these theoretical results to experimentally obtained values. In the two-dimensional case, we present experimentally derived results on random images and a small set of real images.

We show that, for Gaussian smoothing, the strength of a phantom edge increases as the filter scale constant σ increases, while the strength of an authentic edge decreases with σ. From this observation comes the description of these edges as phantom; as we reduce σ and are looking at these edges more closely, they fade away, vanishing altogether at $\sigma = 0$.

Examples of the production, and classification, of phantom edges are given for both real and synthetic imagery, in one and two dimensions. In the two-dimensional experiments, both the Laplacian and second directional derivative edge detection methods are tested. The results of these experiments indicate that phantom edges are indeed produced in significant numbers in practical applications and that the classification procedures described in this paper do detect the phantom edges.

II. Phantom Zero Crossings and Their Detection

Let us consider the zero-crossing edge detection method for the one-dimensional case. This method operates by smoothing the signal with a low-pass filter (usually a Gaussian low-pass filter) and associating edges with the zero crossings of the second derivative of the filtered signal. This process is depicted in Fig. 1. The idea behind

Manuscript received August 19, 1986; revised May 25, 1988. Recommended for acceptance by W. E. L. Grimson. This work was supported in part by the Office of Naval Research under Grant N0014-84-K0504 and in part by the Joint Services Electronics Program.

The author is with the Division of Applied Sciences, Harvard University, Cambridge, MA 02138.

IEEE Log Number 8823859.

0162-8828/89/0100-0043$01.00 © 1989 IEEE

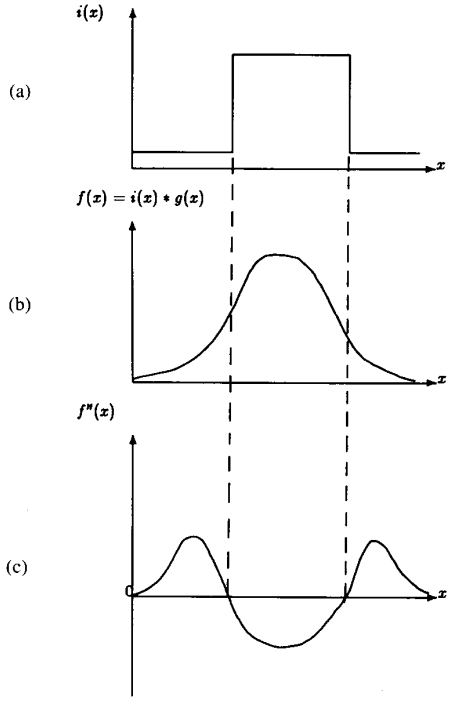

Fig. 1. (a) A one-dimensional step signal. (b) The signal after Gaussian smoothing. (c) The second derivative of the smoothed signal.

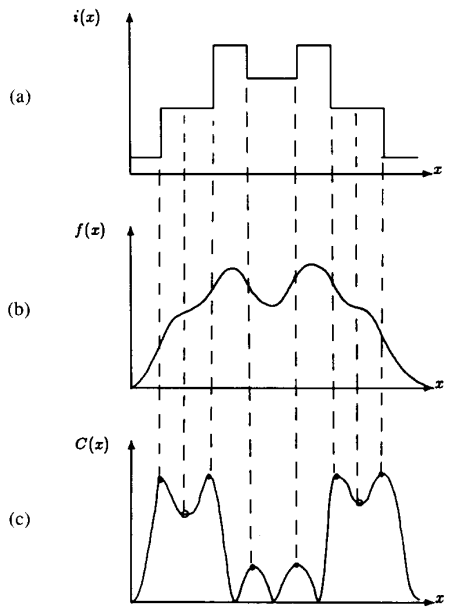

Fig. 2. (a) A one-dimensional step signal. (b) The signal after Gaussian smoothing. (c) The contrast (magnitude of the first derivative) of the smoothed step signal. Its extrema correspond to edges (both phantom and authentic).

the zero-crossing method is that the zeros of the second derivative of a function localize the extremal points of the first derivative of the function. Since edges can be thought of as points where the magnitude of the first derivative of the function is a local maximum, the zeros of the second derivative can localize these edges. A problem with this method arises, however, since the zeros of the second derivative localize the minima of the magnitude of the first derivative, as well as the maxima. The minima of the magnitude of the first derivative cannot be thought of as localizing intensity edges, but rather localize points that are as non-edge-like as possible. Therefore, since the zeros of the second derivative localize both maxima and minima of the magnitude of the first derivative, one cannot assume that all zeros of the second derivative of the smoothed intensity signal correspond to edges. Some of the zeros, those that correspond to minima of the magnitude of the first derivative of the smoothed signal, are not edges at all. We will call these minima *phantom edges*, and the maxima *authentic edges*, and they are defined as follows.

Definition 1: An edge of the smoothed intensity function $f(x)$ is an authentic edge if $|(df)/(dx)|$ is a maximum.

Definition 2: An edge of the smoothed intensity function $f(x)$ is a phantom edge if $|(df)/(dx)|$ is a minimum.

An example of the relationship between the signal and the location of phantom and authentic edges is given in Fig. 2. It can be observed from this example that phantom edges are produced whenever there is a double step in the intensity signal.

Phantom edges as we have defined them have been observed in biological vision systems. Richter and Ullman [11] demonstrated the existence of cells in the visual cortex of both cats and monkeys that respond to the phantom edge found in the center of a double step. This was taken by them as evidence of zero-crossing detection. Their study also observed cells which responded to only the authentic edges, indicating that the visual cortex has some means of distinguishing between phantom and authentic edges. They propose some mechanisms by which this distinction could be made, based on thresholding the edge contrast or on spatial coincidence of edges at different scales, but conclude that these mechanisms are not sufficient for eliminating the phantom edges and suggest that further psychophysical and physiological experimentation is needed to determine how the human visual system handles the phantom edges. In this paper, we provide a way of handling phantom edges which the psychophysicists and physiologists may well find in mammalian vision systems.

Edges are most commonly used as primitive features to be input to higher-level vision modules, such as scene segmentation, motion detection, and stereo depth measurement. These modules assume that the edges produced by the edge detection module are related to physically relevant changes in the image intensity. It is evident that the phantom edges detected by zero-crossing edge detectors are only weakly related to significant changes in the image intensity pattern. For this reason, it is important that one be able to distinguish between phantom and authentic

edges so that only the authentic edges may be passed on to subsequent vision modules. In one dimension, the classification of edges as phantom or authentic is easily accomplished by applying the definition of a phantom or authentic edge. We have defined an authentic edge as an edge for which the magnitude of the first derivative of the filtered signal is a maximum. This is equivalent to requiring that the following condition be true:

$$\frac{df}{dx}\frac{d^3f}{dx^3} < 0. \tag{1}$$

Similarly, a phantom edge is indicated if

$$\frac{df}{dx}\frac{d^3f}{dx^3} > 0. \tag{2}$$

If $(df/dx)(d^3f/dx^3) = 0$, we say there is no edge, as either the contrast $|(df/dx)|$ is zero or (d^3f/dx^3) is zero, in which case we do not have a zero crossing of (d^2f/dx^2). This procedure for distinguishing between authentic phantom edges is seen to be similar to the process of *nonmaximum suppression* [2], which is used in methods which localize edges as maxima in the magnitude of the first derivative of the smoothed signal to determine where the maxima occur. Note that these methods automatically weed out the phantom edges, as only maxima in the magnitude of the first derivative are searched for.

It is easily seen that phantom edges can also occur in the case of two-dimensional zero-crossing edge detectors. The natural extension of the one-dimensional case to the two-dimensional case is to consider edges as points at which the magnitude of the first derivative along the gradient direction is a maximum. This edge detection scheme can be implemented in a zero-crossing algorithm by associating edges with the zero crossings of the second directional derivative along the gradient (of $f(x)$) direction [2], [5], [13]. However, these zero crossings occur at both maxima and minima of the first derivative along the gradient. Thus, this zero-crossing method will produce phantom edges in the same fashion as did the one-dimensional zero-crossing edge detection scheme. Fortunately, the phantom edge can be distinguished from the authentic edges in the same manner as was done in the one-dimensional case. Let $\hat{n}$ be the direction of the gradient of the smoothed function $f(x, y)$. That is, $\hat{n} = \nabla f/|\nabla f|$. Let n be a parameter along this direction. Then the second directional derivative of $f(x, y)$ in the gradient direction is given by

$$\frac{\partial^2 f}{\partial n^2} = \frac{f_x^2 f_{xx} + 2f_x f_y f_{xy} + f_y^2 f_{yy}}{|\nabla f|^2} \tag{3}$$

where $|\nabla f| \neq 0$ and the subscript indicates differentiation [i.e., $f_x = (\partial f/\partial x)$]. Phantom and authentic edges can be distinguished by checking the sign of the following quantity, which indicates whether the edge is a maximum or a minimum of $(\partial f/\partial n)$:

$$\chi = \frac{\partial f}{\partial n}\frac{\partial^3 f}{\partial n^3}. \tag{4}$$

If χ is positive, the edge is phantom. If χ is negative, the edge is authentic, and if χ is zero, we say there is no edge. The derivatives in the expression above involving n can be expressed as derivatives in x, y, yielding

$$\chi = \frac{f_x^3 f_{xxx} + 3f_x f_y^2 f_{xyy} + 3f_x^2 f_y f_{xxy} + f_y^3 f_{yyy} + (f_x^2 + f_y^2)(f_{xy}^2 - f_{xx}f_{yy})}{f_x^2 + f_y^2}. \tag{5}$$

In two dimensions, the zero-crossing edge detection schemes are not limited to use of the second directional derivative along the gradient direction. Any second-order differential operator can be used to indicate the presence of an edge. A common choice of such a second-order differential operator is the Laplacian. The Laplacian of the smoothed intensity function is given by $\nabla^2 f = f_{xx} + f_{yy}$. This operator is obviously much simpler than the second directional derivative operator and is linear as well. Furthermore, it does not have the problem with determining the gradient direction that the second directional derivative scheme has for small $|\nabla f|$ values. These considerations account in part for the great popularity of the Laplacian operator at present in computational vision over the second directional derivative operator. However, the Laplacian edge detector does not localize edges as well as the second directional derivative operator in regions where the edge is highly curved, such as corners [1], [5]. The Laplacian operator is best thought of in the vision context as a useful approximation to the second directional derivative operator. These two operators give similar results when the curvature of the edges is low.

It is evident that, because the Laplacian edge detection method is a zero-crossing method, it will produce phantom edges. However, classifying edges as phantom or authentic is problematic, as it cannot be said that the zeros of $\nabla^2 f$ correspond to maxima or minima of any contrast type of function. Thus, it does not suffice simply to classify Laplacian edges based on a nonmaximum suppression type of process. We can proceed in two ways. The first is to acknowledge that the Laplacian operator is an approximation (usually good) to the second directional derivative along the gradient and use as a classification variable the following:

$$\chi = \frac{\partial(\nabla^2 f)}{\partial n}\frac{\partial f}{\partial n} = \nabla(\nabla^2 f) \cdot \nabla f. \tag{6}$$

If this variable χ is positive, we say the edge is a phantom. If χ is negative, we say the edge is authentic. If χ is zero, we say there is no edge. The second way in which we can proceed is to note that the Laplacian of f is the divergence of the vector field ∇f. The requirement that $\nabla^2 f$ be zero at an edge implies that the divergence of the

gradient of f is zero at an edge, indicating that the gradient field at these points is in a sense stationary or extremal. Since the gradient has both a magnitude and a direction, its divergence will consist of a magnitude change part and a direction change part. We show in the Appendix that the Laplacian of a function can be expressed as follows:

$$\nabla^2 f = \frac{\partial^2 f}{\partial n^2} + |\nabla f| \kappa \tag{7}$$

where κ is the curvature of the level crossing of $f(x, y)$ through the point in question. It is seen that these two components of the Laplacian correspond to the "magnitude change" and "direction change" part of the divergence of ∇f. If the direction of ∇f is not changing, the curvature of the level crossings of f is zero, leaving only the second directional derivative. If the magnitude of ∇f is not changing, then the second directional derivative of f is zero, leaving only the curvature term. Zeros of curvature, however, do not correspond to what one would perceive to be an edge. In fact, zeros of curvature of the level crossings of f tend to form loci that lie perpendicular to the gradient when the gradient magnitude is constant. This implies that only the magnitude change part of the Laplacian contributes to the "edginess" of a zero crossing, while the direction change part contributes only a noise or distortion component. This distortion is manifest in a deviation of the edge location from the ideal location. This deviation was investigated in detail by Berzins [1]. Thus, in determining the authenticity of a zero crossing of the Laplacian filtered signal, one should examine only the magnitude change part. That is, the same classification formula as was used in the second directional derivative case (4) should be used in the Laplacian case as well. In practice, however, the classification formula given as (6) may be more appropriate, due to the fact that the quantity $\nabla^2 f$ is already available, and the second directional derivative need not be computed. If (6) is used, then one may expect possible errors in classification in those regions of high curvature of the level crossings of $f(x, y)$. Of course, the positions of the edges obtained will be in error as well in these regions.

The classification of the zero crossings of the $\nabla^2 G$ filtered image given by (6) was also suggested by Berzins [1]. However, his explanation of the origin of the phantom, or spurious, edges as being due to the nonlinearity of the intensity along a step edge, and to the approximation of the second directional derivative operator by the Laplacian, is seen to be incorrect. Phantoms edges arise with the second directional derivative operator, as well as with the Laplacian operator, so that the approximation of the second directional derivative operator by the Laplacian cannot be blamed for the production of phantom edges. Furthermore, phantom edges can occur when the intensity along a step edge is constant, as in the case of the two-dimensional double step (see Figs. 4 and 5). Thus, the nonlinear intensity variation along a step cannot blamed for the production of phantom edges. We have shown in this paper that the cause of the phantom or spurious edges lies in the zero-crossing detectors both maxima and minima in the magnitude of the gradient, while only maxima of the gradient magnitude correspond to edges.

III. Significance of the Phantom Zero Crossings

A question that naturally arises is, are the phantom zero crossings significant in that their strengths and density are comparable to those of authentic zero crossings? In this section, we endeavor to answer this question.

Let us, for the purposes of clarity in our exposition, make the following definitions.

Definition 3: The contrast of an edge of a function $f(x)$ is the magnitude of the first derivative of $f(x)$ at the edge. That is, $C(x) = |f_x|$.

Definition 4: The strength of an edge of a function $f(x)$ is the square of the contrast. That is, $S(x) = |f_x|^2$.

Recall that authentic edges correspond to maxima of $|(df/dx)|$, and phantom edges correspond to minima of $|(df/dx)|$. From this, we can infer the following theorem.

Theorem 1: The contrast of a phantom edge that lies between two authentic edges (with no other edges between them) is less than the contrast of either of the two authentic edges.

Proof: The proof follows from the fact that a minimum of a function cannot have a higher value than an adjacent maximum.

This theorem implies another.

Theorem 2: If the contrast of a nonconstant function goes to zero at the end points of an interval, then the average density of the phantom edges of that function in the interval is less than the average density of the real edges in the interval.

Proof: Recall that the definition of the contrast of an edge implies that the contrast of a function is always nonnegative. Hence, the contrast at the boundary points of the interval is a global minimum if $(df(x)/dx) = 0$ at these points. But since $(df(x)/dx) = 0$, these minima do not correspond to edges. Since the function $f(x)$ is nonconstant, the mean value theorem of elementary calculus implies that its contrast has at least one extremum in the interval. Since the end points are both global minima, this extremum must be a maximum. It is evident that maxima and minima must alternate in an interval. Thus, because the end points of the interval are minima and there is at least one extremum in the interval, there is one more maximum in the interval than the number of minima. Thus, the density of authentic edges in the interval is greater than the density of phantom edges in the interval.

The differences in the density of phantom edges and authentic edges is actually greater than implied by the above theorem since a fraction of the minima inside the interval may actually be global minima, for which $(df(x)/dx) = 0$, and hence do not correspond to edges. Thus, the number of phantom edges is, in general, smaller than the number of minima of (df/dx). The number of

authentic edges is equal to the number of maxima of (df/dx). The worst case phantom edge production occurs in a staircase function, where the number of phantom zero crossings is equal to the number of authentic zero crossings minus one. In this situation, all of the minima of (df/dx) in the interval are nonglobal and hence correspond to (phantom) edges.

Based on the fact that phantom edges correspond to minima of the contrast and authentic edges correspond to maxima of the contrast, it is tempting to propose a theorem that states something like that the average contrast (or equivalently average contrast) of authentic edges is always greater than the average contrast of phantom edges. However, one cannot do this since not all minima of the contrast correspond to (phantom) edges. Thus, one can have a few phantom edges, all of which have contrast less than an equal number of authentic edges, and a very large number of authentic edges which have very low contrast (but are associated only with global, nonedge minima). In this case, the average phantom edge contrast can be much higher than the average authentic edge contrast, and hence, thresholding of the contrast will not serve to distinguish between phantom and authentic edges. In practice, however, most of the minima are nonglobal and can thus be associated with phantom edges. Hence, in this case, the phantom edges will, on the average, have a lower contrast than the authentic edges. Later in this section, we will demonstrate this for Gaussian distributed random functions.

The strength of the edges of a function $f(x)$ that is obtained by filtering another function $i(x)$ with the Gaussian low-pass filter,

$$g(x) = \frac{1}{\sigma\sqrt{2\pi}} e^{-x^2/2\sigma^2}, \qquad \sigma > 0, \tag{8}$$

exhibits an interesting dependence on the smoothing parameter σ. This property is illustrated by the following theorem.

Lemma 1: The Gaussian smoothed function $f(x)$ and its derivatives are solutions of a diffusion-type equation [6], [15]:

$$\frac{\partial^2 f}{\partial x^2} = \frac{1}{\sigma}\frac{\partial f}{\partial \sigma}. \tag{9}$$

In two dimensions, we have a similar result.

Lemma 2: The Gaussian smoothed function $f(x, y)$ and its derivatives are solutions of a diffusion-type equation:

$$\nabla^2 f = \frac{1}{\sigma}\frac{\partial f}{\partial \sigma}. \tag{10}$$

Theorem 3: The strength $S(x) = |(df/dx)|^2$ of a phantom edge of a Gaussian smoothed function increases with an increase in the smoothing parameter σ. The strength of an authentic edge of a Gaussian smoothed function decreases with an increase in the smoothing parameter σ.

Proof: The derivative of the strength with respect to σ is given by $S_\sigma = 2f_x f_{x\sigma}$. With the above lemma, we can show that $f_{x\sigma} = (1/\sigma)f_{xxx}$. Thus, the sign of S_σ is then given by

$$\text{sgn}\,(S_\sigma) = \text{sgn}\,(f_x f_{xxx}) = \text{sgn}\,(\chi). \tag{11}$$

Along a contour in scale space [14], [15] (i.e., as we track the position of a zero crossing as σ changes continuously) parameterized by arc length s (assumed to be a monotonically increasing function of σ so that $\partial s/\partial\sigma > 0$), we have

$$S_s = S_x x_s + S_\sigma \sigma_s. \tag{12}$$

Since $\text{sgn}\,(\sigma_s) = +1$ and $S_x = 2f_x f_{xx} = 0$ along a zero crossing, we have that

$$\text{sgn}\,(S_s) = \text{sgn}\,(S_\sigma) = \text{sgn}\,(f_x f_{xxx}). \tag{13}$$

From this equation, and (1) and (2), it follows that S_s is positive for phantom edges and negative for authentic edges. Since edge contrast and edge strength are monotonically related, it follows that the contrast of a phantom edge increases with increasing scale as well.

A similar theorem holds in the two-dimensional case.

Theorem 4: Let $f(x, y)$ be a function arising from the Gaussian low-pass filtering of an arbitrary function $i(x, y)$. The strength of $f(x, y)$ (i.e., $|\nabla f|^2$) at a zero of $\nabla^2 f$ then obeys the following equation:

$$\text{sgn}\,(\chi) = \text{sgn}\left(\nabla(\nabla^2 f)\cdot\nabla f\right) = \text{sgn}\left(\frac{\partial|\nabla f|^2}{\partial\sigma}\right). \tag{14}$$

The proof of this theorem follows the same reasoning as the proof of its one-dimensional counterpart.

For a piecewise constant (step edge) signal, increasing σ is equivalent to decreasing the distance between steps, so that we can say that the strength of a phantom edge increases as the distance between it and its two adjacent authentic edges decreases. Clearly, at some point as we increase σ, the strength of the phantom edge will have increased, and its adjacent authentic edges will have weakened, so that their strengths are equal. At this point, the strength of the phantom edge cannot increase any longer with σ, nor can the contrast of the authentic edges decrease any longer. Thus, the phantom zero crossing and the authentic edges must annihilate each other and cease to exist at higher values of σ. This phenomenon will not be studied in this paper, but is analyzed in detail in [3], [4]. In those papers, it is shown that the shape of the scale map contours near such annihilation points is parabolic, and that, in addition, an authentic edge can actually turn into a phantom edge as the scale increases.

The change in contrast over scale provides an alternative means for classifying an edge as authentic or phantom. This has the advantage over the single-scale classification in that only first derivatives (in σ) are required, as opposed to the third derivatives (in x) required in the single-scale classification process. There are some problems with implementing a scale-space classification, how-

ever. One problem is that an authentic edge can turn into a phantom edge as scale increases [3], [4]. This may result in an uncertain classification for an edge that is near to such a transformation point in scale space. One can perform a consistency check to determine whether or not this is the case by examining the classification of two edge points that lie on the same scale map contour, but at two slightly different scales. If they have differing classifications, then one should be wary of these classifications. Furthermore, obtaining the derivative of the contrast with respect to σ may be difficult, or computationally expensive, as two or more filterings of the signal, done at slightly different σ values, must be performed.

We have seen that, in general, the contrast of phantom edges is less than the contrast of authentic edges, and that the number, or density, of phantom edges is also less than that of authentic edges. However, we do not have as yet any feel for how much weaker, or less dense, the phantom edges are compared to the authentic edges. In order to make quantitative statements about this, we need to assume a model for the signal. For the purposes of this paper, we will assume that the signal is a segment of a normally distributed stationary random function. While this model may not accurately model most one-dimensional signals found in computer vision applications, it does allow us to obtain exact results for the relative contrasts and densities of the two classes of zero crossings in the one-dimensional case. Unfortunately, closed-form solutions cannot be obtained for the two-dimensional case.

The following theorems provide expressions for P_p, the probability of an edge being a phantom, and P_a, the probability of an edge being authentic, as well as for the ratio of the expected contrast of a phantom edge to the expected contrast of an authentic edge, all under the assumption that $f(x)$ is a normally distributed random function, with autocorrelation function $\psi(\tau)$ with τ being the autocorrelation lag.

Theorem 5: If $f(x)$ is a normally distributed random function, with autocorrelation function $\psi(\tau)$, then the probability of an edge being a phantom edge is given by

$$P_p = \frac{(1 - a)}{2} \tag{15}$$

where

$$a = \frac{-\psi^{(4)}(0)}{\sqrt{\psi^{(2)}(0)\,\psi^{(6)}(0)}}. \tag{16}$$

The probability of an edge being an authentic edge is given by

$$P_a = 1 - P_p = \frac{(1 + a)}{2}. \tag{17}$$

Proof: An edge occurs when f_{xx} crosses zero. The probability of a zero crossing of f_{xx} being phantom is

$$P_p = \Pr(\chi > 0 \,|\, f_{xx} = 0) = \Pr(f_x f_{xxx} > 0 \,|\, f_{xx} = 0)$$

$$= \frac{\Pr(f_x f_{xxx} > 0, f_{xx} = 0)}{\Pr(f_{xx} = 0)}. \tag{18}$$

Let $y_1 = f_x$, $y_2 = f_{xx}$, and $y_3 = f_{xxx}$; then, since $f(x)$ is a normally distributed random function, the joint probability density of y_1, y_2, and y_3 can be written as

$$Z(\vec{y}) = \frac{1}{(2\pi)^{3/2}\sqrt{|M|}}\, e^{-(1/2\vec{y}^T M^{-1}\vec{y})} \tag{19}$$

where M is the covariance matrix of $\vec{y}$ (we assume that y_1, y_2, and y_3 are zero mean) and $|M|$ is the determinant of M:

$$M = \begin{bmatrix} -\psi^{(2)}(0) & 0 & -\psi^{(4)}(0) \\ 0 & \psi^{(4)}(0) & 0 \\ -\psi^{(4)}(0) & 0 & -\psi^{(6)}(0) \end{bmatrix}. \tag{20}$$

Now, P_p can be written

$$P_p = \frac{\Pr(y_1 y_3 > 0, y_2 = 0)}{\Pr(y_2 = 0)}. \tag{21}$$

We can write the probability of finding y_1 in an interval $(y_1, y_1 + dy_1)$, y_2 in an interval $(y_2, y_2 + dy_2)$, and y_3 in an interval $(y_3, y_3 + dy_3)$ as

$$Z(y_1, y_2, y_3)\, dy_1\, dy_2\, dy_3. \tag{22}$$

For $y_2 = 0$, we can write $dy_2 = |y_3|\, dx$; hence, we have that

$$\Pr(y_2 = 0) = \int_{-\infty}^{\infty}\int |y_3| Z(y_1, 0, y_3)\, dy_1\, dy_3\, dx \tag{23}$$

$$= 2\left(\int_0^{\infty}\int y_3 Z(y_1, 0, y_3)\, dy_1\, dy_3\, dx - \int_{-\infty}^{0}\int_0^{\infty} y_3 Z(y_1, 0, y_3)\, dy_1\, dy_3\, dx\right), \tag{24}$$

and similarly,

$$\Pr(y_1 y_3 > 0, y_2 = 0) = 2\int_0^{\infty}\int y_3 Z(y_1, 0, y_3)\, dy_1\, dy_3\, dx. \tag{25}$$

Thus, we have the following expression for P_p:

$$P_p = \frac{\int_0^\infty \int_0^\infty y_3 Z(y_1, 0, y_3)\, dy_1\, dy_3}{\int_0^\infty \int_0^\infty y_3 Z(y_1, 0, y_3)\, dy_1\, dy_3 - \int_{-\infty}^0 \int_0^\infty y_3 Z(y_1, 0, y_3)\, dy_1\, dy_3}. \tag{26}$$

Similarly, the probability of an authentic zero crossing, P_a, is given by

$$P_a = \frac{\int_{-\infty}^0 \int_0^\infty y_3 Z(y_1, 0, y_3)\, dy_1\, dy_3}{\int_0^\infty \int_0^\infty y_3 Z(y_1, 0, y_3)\, dy_1\, dy_3 - \int_{-\infty}^0 \int_0^\infty y_3 Z(y_1, 0, y_3)\, dy_1\, dy_3}. \tag{27}$$

Let $\mu = \frac{1}{2}M^{-1}$. Then, we have

$$Z(y_1, 0, y_3) = \left[\frac{1}{(2\pi)^{3/2}\sqrt{|M|}}\right] \cdot e^{-(\mu_{11}y_1^2 + 2\mu_{13}y_1y_3 + \mu_{33}y_3^2)}. \tag{28}$$

If we make the change of variables $t_1 = y_1\sqrt{\mu_{11}}$, $t_3 = y_3\sqrt{\mu_{33}}$, then

$$Z(t_1, t_3) = Ke^{-(t_1^2 + 2at_1t_3 + t_3^2)} \tag{29}$$

where $a = (\mu_{13})/(\sqrt{\mu_{11}\mu_{33}})$ and $K = 1/\sqrt{\mu_{11}\mu_{33}(2\pi)^3|M|}$. The value of a can be expressed in terms of the elements of M to yield

$$a = -\frac{\psi^{(4)}(0)}{\sqrt{\psi^{(2)}(0)\,\psi^{(6)}(0)}}. \tag{30}$$

We can thus write

$$\int_0^\infty \int_0^\infty y_3 Z(y_1, 0, y_3)\, dy_1\, dy_3 = \frac{K}{\sqrt{\mu_{33}}} \int_0^\infty \int_0^\infty t_3 e^{-(t_1^2 + 2at_1t_3 + t_3^2)}\, dt_1\, dt_3. \tag{31}$$

Rice [10] shows that the integral in the above equation evaluates to $\sqrt{\pi}/[4(1 + a)]$. Similarly,

$$-\int_{-\infty}^0 \int_0^\infty y_3 Z(y_1, 0, y_3)\, dy_1\, dy_3 = \frac{K}{\sqrt{\mu_{33}}} \int_0^\infty \int_0^\infty t_3 e^{-(t_1^2 - 2at_1t_3 + t_3^2)}\, dt_1\, dt_3 = \frac{K\sqrt{\pi}}{4\sqrt{\mu_{33}}(1 - a)}. \tag{32}$$

The above equations, along with the expressions (18) and (19) for P_p and P_a, yield

$$P_p = \frac{\frac{1}{1 + a}}{\frac{1}{1 + a} + \frac{1}{1 - a}} = \frac{1 - a}{2} \tag{33}$$

and

$$P_a = \frac{\frac{1}{1 - a}}{\frac{1}{1 + a} + \frac{1}{1 - a}} = \frac{1 + a}{2}. \tag{34}$$

If we assume that the input signal is white (i.e., $r(\tau) = \delta(\tau)$) and that the smoothing filter is Gaussian, then the autocorrelation function of the filtered signal is given by

$$\psi(\tau) = \frac{1}{2\sigma\sqrt{\pi}} e^{-r^2/(4\sigma^2)}. \tag{35}$$

By doing a McLaurin series expansion of $\psi(\tau)$ and of $e^{-r^2/(4\sigma^2)}$ it can be seen that the derivatives of $\psi(\tau)$ evaluated at zero are

$$\psi^{(n)}(0) = \frac{(-1)^{(n/2)}n!}{\left(\frac{n}{2}\right)!\, 2^{n+1}\sigma^{n+1}\sqrt{\pi}} \tag{36}$$

for n even and are zero for n odd. From this, we compute that $a = \sqrt{3/5}$, which yields $P_p = 0.113$. Thus, we expect to find that roughly one out of every nine edges is phantom. One can derive the probability of a zero crossing being authentic in a similar fashion; the result is $P_a = 0.887$. The ratio of the density of authentic zero crossings to phantom zero crossings is thus

$$\frac{P_a}{P_p} = \frac{1}{P_p} - 1 = \frac{1 + a}{1 - a} = 7.87. \tag{37}$$

It is evident then that for a normally distributed white ran-

dom signal, when smoothed by a Gaussian low-pass filter, the density of authentic zero crossings is about eight times the density of phantom zero crossings. Note that the ratio of the densities of the authentic and phantom zero crossings is independent of σ.

We will now state the theorem concerning the ratio of the expected contrasts of authentic and nonauthentic zero crossings.

Theorem 6: The ratio of the expected contrast of the authentic edges to the phantom edges of a normally distributed random variable, with autocorrelation function $\psi(\tau)$ is given by

$$\frac{C_a}{C_p} = \left(\frac{1-a}{1+a}\right)\left[1 + \left(\frac{\pi a}{\sqrt{1-a^2} - a\cos^{-1}(a)}\right)\right] \tag{38}$$

where a is given by

$$a = -\frac{\psi^{(4)}(0)}{\sqrt{\psi^{(2)}(0)\,\psi^{(6)}(0)}}. \tag{39}$$

Proof: The expected value of the edge contrast, given that the edge is a phantom edge, can be written

$$C_p = E\{|f_x| \mid f_x f_{xxx} > 0, f_{xx} = 0\}. \tag{40}$$

As before, let $y_1 = f_x$, $y_2 = f_{xx}$, and $y_3 = f_{xxx}$; then C_p can be written in integral form as follows:

$$C_p = \int_{-\infty}^{\infty} |y_1| p(y_1 | y_1 y_3 > 0, y_2 = 0)\, dy_1$$

$$= 2\int_0^{\infty} y_1 p(y_1 | y_3 > 0, y_2 = 0)\, dy_1. \tag{41}$$

The quantity $p(y_1 | y_1 y_3 > 0, y_2 = 0)$ can be expressed as

$$p(y_1 | y_1 y_3 > 0, y_2 = 0) = \frac{p(y_1, y_1 y_3 > 0, y_2 = 0)}{p(y_1 y_3 > 0, y_2 = 0)}. \tag{42}$$

In the proof of the previous theorem, we showed that

$$p(y_1 y_3 > 0, y_2 = 0) = \frac{dx}{(1+a)} = P_p\, dx. \tag{43}$$

Hence,

$$C_p = \frac{2\int_0^{\infty} y_1 p(y_1, y_3 > 0, y_2 = 0)\, dy_1}{P_p\, dx}. \tag{44}$$

Now, $p(y_1, y_3 > 0, y_2 = 0)$ can be expressed, using $dy_2 = |y_3|\, dx$, as

$$p(y_1, y_3 > 0, y_2 = 0)$$

$$= \left(\int_0^{\infty} y_3 Z(y_1, 0, y_3)\, dy_3\right) dx. \tag{45}$$

Thus, we have

$$C_p = \frac{2\left(\int_0^{\infty}\int_0^{\infty} y_1 y_3 Z(y_1, 0, y_3)\, dy_1\, dy_3\right) dx}{P_p\, dx}. \tag{46}$$

From the definition of $Z(\vec{y})$ and making the substitutions $t_1 = y_1\sqrt{\mu_{11}}$, $t_3 = y_3\sqrt{\mu_{33}}$ as before, we obtain

$$C_p = \frac{\dfrac{K}{\sqrt{\mu_{11}\mu_{33}}}\displaystyle\int_0^{\infty}\int t_1 t_3 e^{-(t_1^2 + 2a t_1 t_3 + t_3^2)}\, dt_1\, dt_3}{P_p}. \tag{47}$$

Rice [10] provides the solution for the integral in the expression above, and we can write

$$C_p = \frac{\csc^2(\varphi)[1 - \varphi\cot(\varphi)]}{P_p} \tag{48}$$

where $\varphi = \cos^{-1}(a)$. The value of the parameter a can be expressed in terms of the elements of the autocorrelation matrix M as follows:

$$a = -\frac{\psi^{(4)}(0)}{\sqrt{\psi^{(2)}(0)\,\psi^{(6)}(0)}}. \tag{49}$$

One can easily show that

$$\csc^2(\varphi) = \frac{1}{1-a^2}, \quad \cot(\varphi) = \frac{a}{\sqrt{1-a^2}} \tag{50}$$

Thus, we can write, after some algebra

$$C_p = \frac{\sqrt{1-a^2} - a\cos^{-1}(a)}{1-a}. \tag{51}$$

Similarly, it can be shown that the expected contrast of an authentic zero crossing is obtained simply from the expression for C_p by changing the sign of a. Doing this yields

$$C_a = \frac{\sqrt{1-a^2} - a\cos^{-1}(a) + \pi a}{1+a}. \tag{52}$$

Hence, the ratio of the expected contrast of the authentic zero crossings to the expected contrast of the phantom zero crossings is given by

$$\frac{C_a}{C_p} = \left(\frac{1-a}{1+a}\right)\left[1 + \left(\frac{\pi a}{\sqrt{1-a^2} - a\cos^{-1}(a)}\right)\right]. \tag{53}$$

For the value of a determined earlier, this ratio works out to be $C_a/C_p = 3.155$. Thus, the authentic edges are, on the average, about three times stronger than the phantom edges.

We have shown that, for the case of white, normally distributed random signals, the phantom edges are fewer (by a factor of about nine) and weaker (by a factor of about three) than the authentic edges. One cannot conclude from this that the phantom edges are not significant,

however. There may be phantom edges whose contrast is greater than some authentic edges, so that, while thresholding will get rid of most of the phantom edges, it will not eliminate all of them and will eliminate some of the authentic edges. Note that some of the authentic edges may be due to noise and thus may not correspond to significant image detail. The edge classification procedure will therefore not remove these noise edges, and some other method must be used to eliminate them (such as thresholding of the edge contrast after the classification process).

IV. Examples of Phantom Edge Production and Classification

Examples of the classification process are shown in Figs. 3–7. Fig. 3 depicts the classification of the zero crossings of the second derivative of a smoothed one-dimensional Gaussian noise signal. The zero crossings classified as authentic are represented by solid vertical lines, while the phantom zero crossings are represented by dashed vertical lines. Notice that the phantom zero crossings occur whenever there is a double step in the signal. Figs. 4(a) and 5(a) are computer-generated images of repetitive intensity step functions. Figs. 6(a) and 7(a) are images of typical laboratory scenes obtained with a video camera. The set of all zero crossings of the filtered image are shown in part (b) of Figs. 4–7. These include both the authentic and the phantom zero crossings. In Figs. 4 and 7, the Laplacian operator was used, while in Figs. 5 and 6, the second directional derivative along the gradient operator was used. The value of σ for the Gaussian filter was ten pixels in all of the two-dimensional experiments described in this paper. The classification of the zero crossings is given in part (c) of the figures. The authentic zero crossings are in black, while the phantom zero crossings are in white. Finally, part (d) of the figures shows just the zero crossings that were classified as authentic. Note that, in the synthetic images, the classification scheme performed correctly, as it classified as phantoms those zero crossings which did not correspond to any of the intensity steps in the original image. Note also that these phantom zero crossings arose when along a gradient track there were consecutive changes in image intensity with the same sense. In the case of the video camera data, it is interesting to note the relative abundance of the phantom zero crossings, as well as where they occur. The resulting authentic zero-crossing image is seen to be much cleaner than the image containing all the zero crossings. The phantom zero crossings do not seem to correspond to significant image features, whereas the zero crossings classified as authentic do, in general, correspond to actual image features.

We also ran experiments to generate statistics on the relative frequency and contrasts of the phantom and authentic zero crossings. This was done to check the mathematical analysis done in Section III for the one-dimensional case and to provide a feeling for the two-dimensional case, for which the mathematical analysis was not possible. The results of these experiments are summarized in Table I. The results for the case of the one-dimensional Gaussian signal ($P_p = 0.125$, $C_a/C_p = 2.997$) are close to those predicted by the mathematical analysis of Section IV ($P_p = 0.113$, $C_a/C_p = 3.155$). The results on the two-dimensional images are interesting. They indicate that for typical images the probability of a phantom edge is around 0.15, or one in seven. The contrasts of the phantom edges are on the order of one-seventh to one-tenth the contrast of the authentic edges. It is interesting to note that the frequency and contrast of the phantom edges for a Gaussian noise image are much less than for a typical real image. This indicates that there is a relative abundance of "double-step"-like intensity patterns in real images, as compared to random images. This observation could help to produce more realistic image models by insisting on more double-step intensity patterns in a synthetic image.

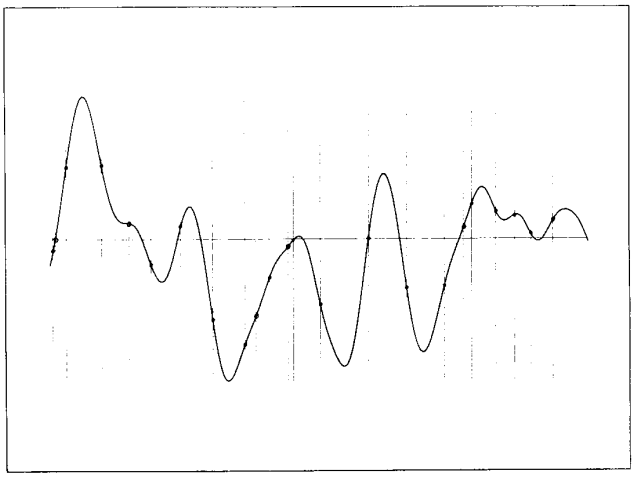

Fig. 3. The classification of the edges of a one-dimensional signal. The locations of authentic edges are indicated by solid vertical lines, while the locations of phantom edges are indicated by dashed vertical lines.

V. Summary

We have demonstrated in this paper that edges produced by the zero-crossing methods do not always correspond to intensity changes in the image. A method for classifying the zero crossings produced by these edge detection schemes as either phantom or authentic was presented.

Experiments were described that supported the claim that phantom zero crossings are common and that demonstrated the efficacy of the classification scheme in distinguishing the phantom zero crossings from the authentic zero crossings.

A probabilistic analysis was performed, under the assumption that the signal was a normally distributed random variable, which showed that, for the case of one-dimensional white noise signals, smoothed by a Gaussian low-pass filter, the density of the authentic zero crossings is roughly eight times that of the phantom zero crossings and that the contrast of authentic zero crossings is, on the average, about three times the contrast of phantom zero crossings.

It was demonstrated that, for the case of zero crossings

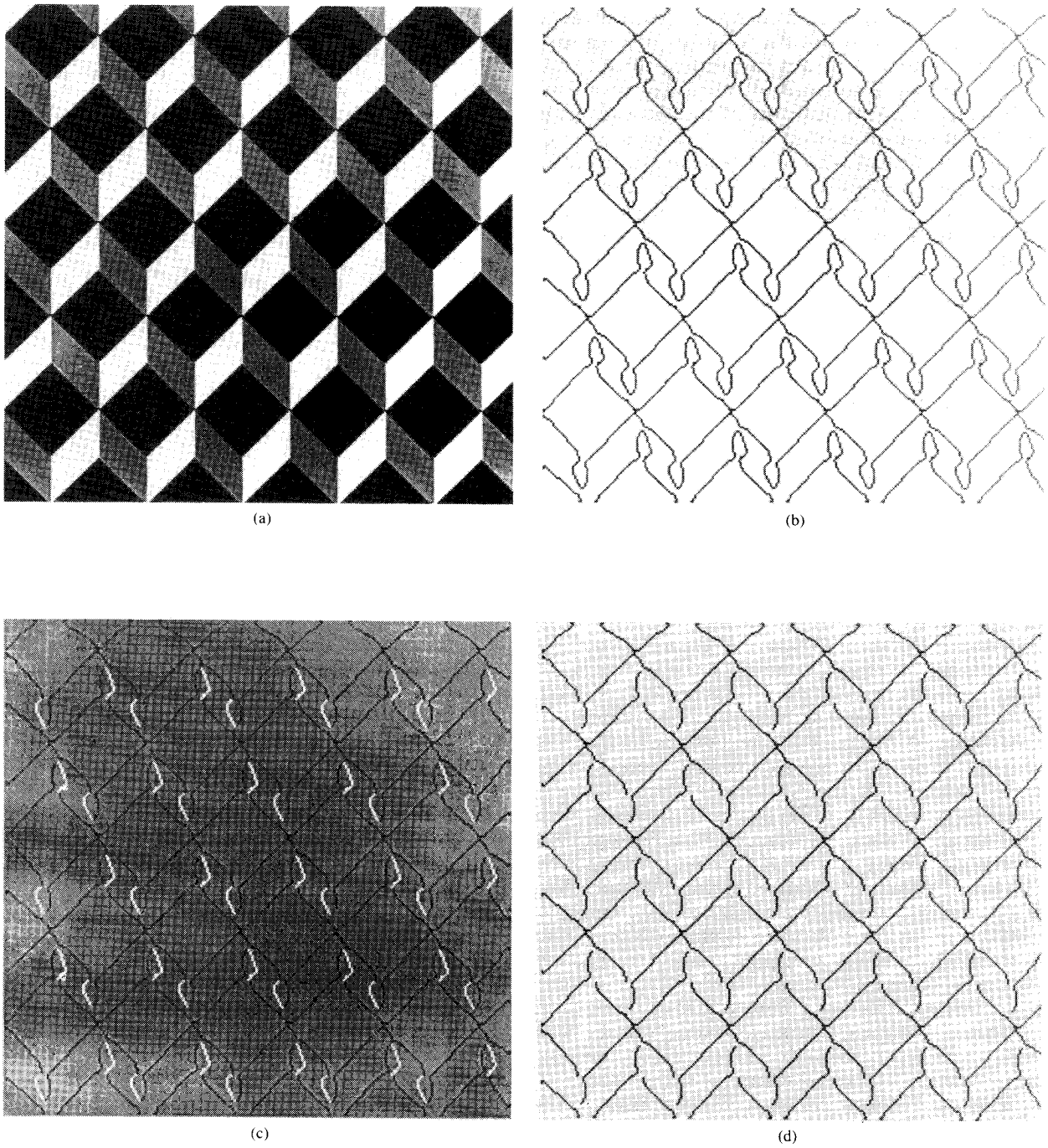

Fig. 4. (a) A synthetic piecewise constant intensity image. (b) The zero crossings of the image after $\nabla^2 G$ filtering. (c) The classification of the zero crossings [using (6)]. White indicates phantom edges, while black indicates the presence of an authentic edge. (d) The authentic edges of the image only.

of $\nabla^2 G$ filtered signals, the contrast of the phantom zero crossings increased with an increase in the filter σ, while the contrast of the authentic zero crossings diminished.

The $\nabla^2 G$ and $(\partial^2 G/\partial n^2)$ zero-crossing edge detection methods are very popular at the present time in the computational vision and image analysis field. Those using these methods should be aware that not all of the edges found by them are authentic edges and that the phantom edges do occur in significant numbers and contrasts in typical images. It is clear that in order to obtain the best

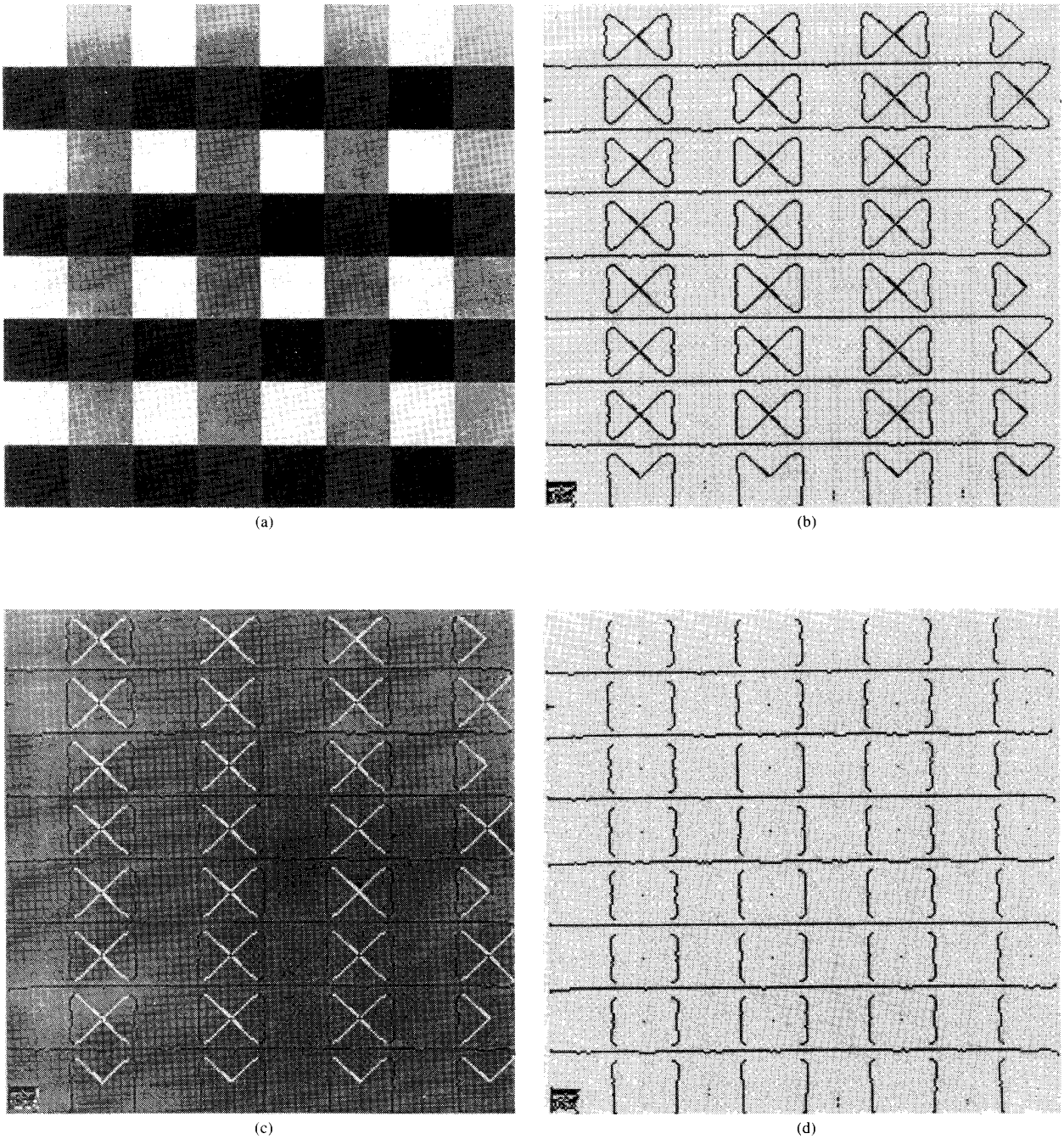

Fig. 5. (a) Another synthetic piecewise constant intensity image. (b) The zero crossings of the image after Gaussian smoothing and application of the second directional derivative along the gradient operator. (c) The classification of the zero crossings. White indicates phantom edges, while black indicates the presence of an authentic edge. (d) The authentic edges of the image only.

performance possible from a given application, such as stereo vision, the phantom edges produced by zero-crossing edge detection algorithms should be detected and discarded. In this paper, we have provided a means for doing so.

Appendix
Decomposition of the Laplacian

In this Appendix, we develop a decomposition of the Laplacian into two parts. If we consider the Laplacian as

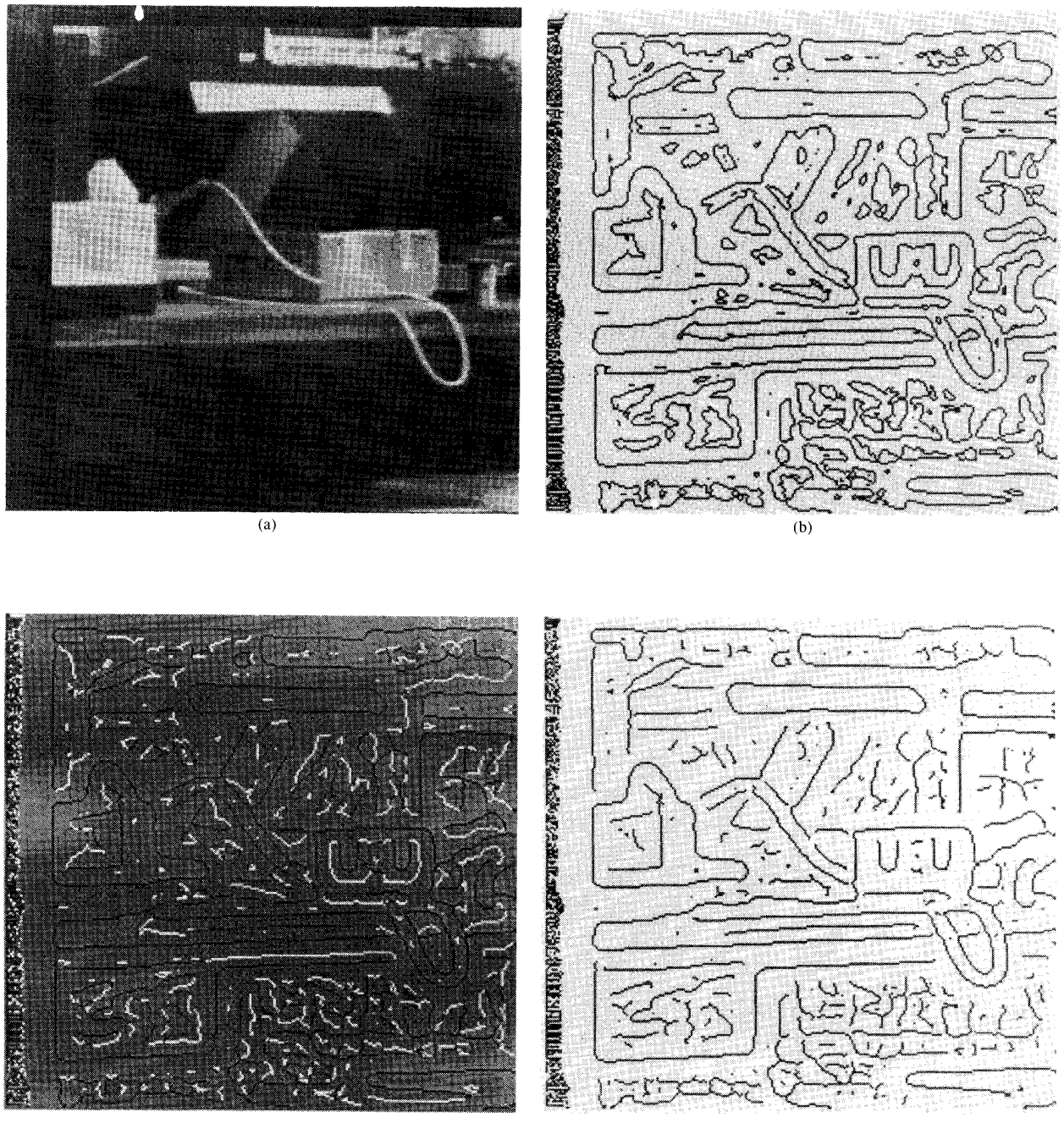

(a) (b) (c) (d)

Fig. 6. (a) An image obtained from a video camera. (b) The zero crossings of the image after Gaussian smoothing and application of the second directional derivative along the gradient operator. (c) The classification of the zero crossings. White indicates phantom edges, while black indicates the presence of an authentic edge. (d) The authentic edges of the image only.

the divergence of a gradient field, these two parts correspond to a "gradient magnitude change" part and a "gradient direction change" part.

We begin by finding an expression for the Laplacian operator in a general curvilinear coordinate system. Let us define a curvilinear coordinate system with basis vectors $\overset{1}{\hat{e}}$, $\overset{2}{\hat{e}}$, and coordinates u^1, u^2 and metric tensor g^{ij}. The basis vectors are related to the coordinate functions by $\overset{1}{\hat{e}} = \nabla u^1$ and $\overset{2}{\hat{e}} = \nabla u^2$. The metric tensor is given by $g^{ij} = \overset{i}{\hat{e}} \cdot \overset{j}{\hat{e}}$ $i, j = 1, 2$. The Laplacian can be expressed in this

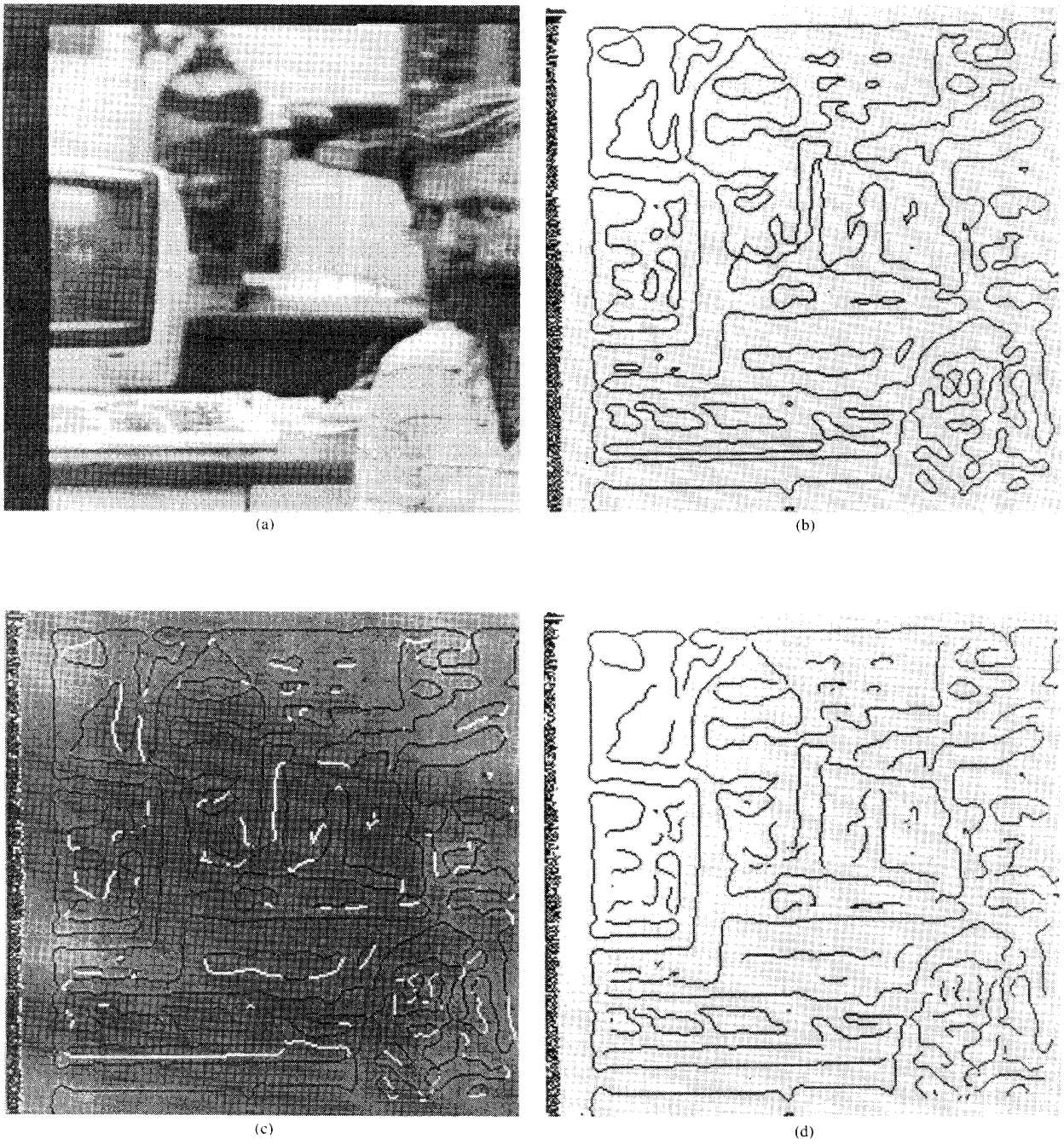

(a) (b) (c) (d)

Fig. 7. (a) An image obtained from a video camera. (b) the zero crossings of the image after $\nabla^2 G$ filtering. (c) The classification of the zero crossings. White indicates phantom edges, while black indicates the presence of an authentic edge. (d) The authentic edges of the image only.

coordinate system with the following (given in many texts on differential geometry, e.g., [12]):

$$\nabla^2 f = \frac{\partial\left(g^{ij}\dfrac{\partial f}{\partial u^j}\right)}{\partial u^i} + \Gamma^k_{ik} g^{ij} \frac{\partial f}{\partial u^j} \tag{54}$$

TABLE I
RESULTS OF CLASSIFICATION EXPERIMENTS

Image Name	Figure 6	Figure 7	Mona Lisa	2D Random	1D Random	Theory.1D
No. Authentic	23629	20074	11504	18841	8829	8949
No. Phantom	3765	3661	2272	1221	1257	1137
No. Edges	27394	23735	13776	20062	10086	10086
Prob. Phantom	0.137	0.154	0.165	0.069	0.125	0.113
C_s/C_p	9.346	7.005	10.054	32.34	2.997	3.155

where the Einstein summation convention is used (i.e., summation is implied over repeated indexes) and the quantity Γ_{ij}^{k}, called the Christoffel symbol of the second kind, is defined in terms of the coordinate basis vectors as follows:

$$\Gamma_{ij}^{k} = \frac{\partial(\overset{s}{\hat{e}}\, g_{is})}{\partial u^{j}} \cdot \overset{k}{\hat{e}}. \tag{55}$$

The expression for the Laplacian expands to

$$\nabla^2 f = \left(\frac{\partial^2 f}{\partial u^i \partial u^j}\right) g^{ij} + \left(\frac{\partial g^{ij}}{\partial u^i} + \Gamma_{ik}^{k} g^{ij}\right) \frac{\partial f}{\partial u^j}. \tag{56}$$

Now let us use as the basis vectors for one curvillinear coordinate system the unit vectors $\vec{n}$ and $\vec{n}_\perp$ that are normal and perpendicular to the curves of constant $f(x, y)$. That is,

$$\overset{1}{\hat{e}} = \nabla u^1 = \frac{1}{|\nabla f|}\left(\frac{\partial f}{\partial x}, \frac{\partial f}{\partial y}\right) = \frac{\nabla f}{|\nabla f|} \tag{57}$$

$$\overset{2}{\hat{e}} = \nabla u^2 = \frac{1}{|\nabla f|}\left(\frac{\partial f}{\partial y}, \frac{-\partial f}{\partial x}\right). \tag{58}$$

We then have that

$$(g^{ij}) = (\overset{i}{\hat{e}} \cdot \overset{j}{\hat{e}}) = I. \tag{59}$$

Let us, following the usual computer vision notation, let $n = u^1$ be the coordinate in the $\vec{n}$ direction, and $n_\perp = u^2$ be the coordinate in the $\vec{n}_\perp$ direction.

It is easily seen that $(\partial f/\partial n_\perp) = 0$ identically since $f(x, y)$ is constant in the direction perpendicular to its gradient. Furthermore, one can show that $(\partial f/\partial n) = |\nabla f|$. Hence, we have

$$\nabla^2 f = \frac{\partial^2 f}{\partial n^2} + \frac{\partial^2 f}{\partial n_\perp^2} + (\Gamma_{11}^{1} + \Gamma_{12}^{2})|\nabla f|. \tag{60}$$

From the definition of the Christoffel symbols, we get that

$$\Gamma_{11}^{1} = \frac{\partial \vec{n}}{\partial n} \cdot \vec{n} \tag{61}$$

and

$$\Gamma_{12}^{2} = \frac{\partial \vec{n}}{\partial n_\perp} \cdot \vec{n}_\perp. \tag{62}$$

Since $(\partial \vec{n}/\partial n)$ and $\vec{n}$ are orthogonal, we have that $\Gamma_{11}^{1} = 0$. We can thus express the Laplacian as

$$\nabla^2 f = \frac{\partial^2 f}{\partial n^2} + \frac{\partial^2 f}{\partial n_\perp^2} + \left(\vec{n}_\perp \cdot \frac{\partial \vec{n}}{\partial n_\perp}\right)|\nabla f|. \tag{63}$$

The last term in the above expression can be expanded using $(\partial \vec{n}/\partial n_\perp) = \nabla \vec{n} \cdot \vec{n}_\perp$ and is given by

$$\left(\vec{n}_\perp \cdot \frac{\partial \vec{n}}{\partial n_\perp}\right)|\nabla f| = \frac{f_y^2 f_{xx} - 2f_x f_y f_{xy} + f_x^2 f_{yy}}{|\nabla f|^2}. \tag{64}$$

Thus, we have

$$\nabla^2 f = \frac{\partial^2 f}{\partial n^2} + \frac{\partial^2 f}{\partial n_\perp^2} + \frac{f_y^2 f_{xx} - 2f_x f_y f_{xy} + f_x^2 f_{yy}}{|\nabla f|^2}. \tag{65}$$

It can be shown (see, for example, [2], [13]) that

$$\frac{\partial^2 f}{\partial n^2} = \frac{f_x^2 f_{xx} + 2f_x f_y f_{xy} + f_y^2 f_{yy}}{|\nabla f|^2}. \tag{66}$$

Substitution into (65) gives

$$\nabla^2 f = f_{xx} + f_{yy} + \frac{\partial^2 f}{\partial n_\perp^2}. \tag{67}$$

Thus, we see that $(\partial^2 f/\partial n_\perp^2) = 0$. This observation (which shows that [13, eq. (4.9)] is in error) is also obtained by noting that $(\partial f/\partial n_\perp)$ is identically zero, and hence so are any of its higher derivatives, including $(\partial^2 f/\partial n_\perp^2)$. We can now write

$$\nabla^2 f = \frac{\partial^2 f}{\partial n^2} + \left(\vec{n}_\perp \cdot \frac{\partial \vec{n}}{\partial n_\perp}\right)|\nabla f|. \tag{68}$$

The quantity $(\vec{n}_\perp \cdot (\partial \vec{n}/\partial n_\perp))$ can be shown to be equal to the curvature κ of the level crossing of $f(x, y)$ through the point (x, y). Hence, we have

$$\nabla^2 f = \frac{\partial^2 f}{\partial n^2} + \kappa|\nabla f|. \tag{69}$$

The above expression for the Laplacian in terms of the second directional derivative along the gradient and an additive curvature term supports the observation, attributed to Kass in [13], that $\nabla^2 f = (\partial^2 f/\partial n^2)$ when the curvature of the level-crossing lines of the intensity function $f(x, y)$ is zero. The above expression also reduces to the form, given in [13],

$$\nabla^2 f = \frac{\partial^2 f}{\partial n^2} + \frac{1}{\rho}\frac{\partial f}{\partial \rho} \tag{70}$$

in polar coordinates when $f(x, y)$ is radially symmetric (and whose level crossings thus have a curvature $\kappa = 1/\rho$).

Acknowledgment

The author would like to thank R. W. Brockett for many informative discussions about the research presented in this paper as well as for making available the facilities of the Harvard Robotics Laboratory to perform the experiments described herein. He would also like to thank A. L. Yuille for his comments regarding the Appendix.

References

[1] V. Berzins, "Accuracy of laplacian edge detectors," *Comput. Vision, Graphics, Image Processing*, vol. 27, pp. 195-210, 1984.
[2] J. Canny, "Finding edges and lines in images," M.S. thesis, Mass. Inst. Technol., Cambridge, MA, 1983.
[3] J. J. Clark, "Singularities of contrast functions in scale space," in *Proc. First Int. Conf. Comput. Vision*, London, UK, pp. 491-495, 1987.
[4] ——, "Singularity theory and phantom edges in scale space," *IEEE Trans. Pattern Anal. Mach. Intell.*, to be published.
[5] R. M. Haralick, "Digital step edges from zero crossings of second directional derivatives," *IEEE Trans. Pattern Anal. Mach. Intell.*, vol. PAMI-6, pp. 58-68, 1984.
[6] R. A. Hummel and B. C. Gidas, "Zero crossings and the heat equation," Div. Comput. Sci., Courant Inst. Math. Sci., New York Univ., Tech. Rep. 111, 1984.

[7] D. Marr and E. C. Hildreth, "Theory of edge detection," *Proc. Roy. Soc. London, Ser. B*, vol. 207, pp. 187-217, 1980.
[8] D. Marr and T. Poggio, "A computational theory of human stereo vision," *Proc. Roy. Soc. London, Ser. B*, vol. 204, pp. 301-328, 1979.
[9] V. S. Nalwa and T. O. Binford, "On detecting edges," *IEEE Trans. Pattern Anal. Mach. Intell.*, vol. PAMI-8, pp. 699-714, 1986.
[10] S. O. Rice, "Mathematical analysis of random noise," *Bell Syst. Tech. J.*, vol. 24, pp. 46-156, 1945.
[11] J. Richter and S. Ullman, "Non-linearities in cortical simple cells and the possible detection of zero crossings," *Biol. Cybernet.*, vol. 53, pp. 195-202, 1986.
[12] J. J. Stoker, *Differential Geometry*. New York: Wiley-Interscience, 1969.
[13] V. Torre and T. Poggio, "On edge detection," *IEEE Trans. Pattern Anal. Mach. Intell.*, vol. PAMI-8, 1986.
[14] A. Witkin, "Scale space filtering," in *Proc. 8th Int. Joint Conf. Artif. Intell.*, Karlsruhe, West Germany, 1983, pp. 1019-1022.
[15] A. L. Yuille and T. Poggio, "Scaling theorems for zero crossings," Mass. Inst. Technol., Cambridge, MA, AI Memo 722, 1983.

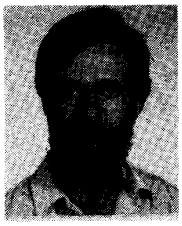

James J. Clark (S'77-M'85) was born in Vancouver, B.C., Canada, in 1957. He received the B.A.Sc. and Ph.D. degrees in electrical engineering from the University of British Columbia, Vancouver, in 1980 and 1985, respectively.

From September 1985 to June 1986 he was a Postdoctoral Fellow and Instructor in the Division of Applied Sciences, Harvard University, Cambridge, MA. Since July 1986, he has been Assistant Professor of Electrical Engineering on the Gordon McKay Endowment in the Division of Applied Sciences at Harvard University. In addition, he is on the faculty of the Harvard/University of Maryland Systems Research Center. His research interests lie in the areas of sensory systems for robotics, analog integrated circuit design, and signal processing.

Dr. Clark was awarded the 1987 IEEE ASSP Paper Award for the best paper in the IEEE TRANSACTIONS ON ACOUSTICS, SPEECH, AND SIGNAL PROCESSING in the digital signal processing area by an author under 30 years old.